Neuromodulatory influences on propagation of brain waves along the unimodal-transmodal gradient

Mäki-Marttunen, V.; Nieuwenhuis, S.T.

Cerebral Cortex, 2025, **35**, bhaf183
https://doi.org/10.1093/cercor/bhaf183
Advance access publication date 15 July 2025
Original Article

Neuromodulatory influences on propagation of traveling waves along the unimodal–transmodal gradient

Verónica Mäki-Marttunen [1,2,*] and Sander Nieuwenhuis[2]

[1]Section for Precision Psychiatry, Oslo University Hospital, Kirkeveien 166, Building 49, 0424 Oslo, Norway
[2]Cognitive Psychology Unit, Institute of Psychology, Leiden University, Wassenaarseweg 52, 2333 AK Leiden, the Netherlands
*Corresponding author: Verónica Mäki-Marttunen, Section for Precision Psychiatry, Oslo University Hospital, Building 49, 0424 Oslo, Norway.
Email: makimarttunen.veronica@gmail.com

Understanding the factors underlying brain activity fluctuation is important to understand the flexible nature of the brain and cognition. Growing evidence indicates that functional magnetic resonance imaging (fMRI) activity travels as waves around global signal peaks following a unimodal–transmodal gradient. This may explain the organization of brain activity into functional networks, but why the strength of integration between networks fluctuates is uncertain. Given that arousal-related neuromodulatory systems affect network integration and that traveling waves are modulated by arousal, we aimed to assess the hypothesis that an increase in neuromodulatory tone can affect network integration by modulating the speed of propagation of traveling waves. We tested this hypothesis using pharmacological fMRI/pupil measurements during rest and tasks. Atomoxetine, which increases extracellular catecholamine levels, was associated with faster traveling waves, and faster traveling waves correlated with more network integration. We also examined temporal variations in pupil size, a signature of transient changes in neuromodulatory activity, and found that the periods of traveling waves were characterized by larger pupil size. Our results suggest that neuromodulatory tone affects traveling wave propagation, and that this arousal-modulated propagation shapes integrated functional connectivity features, highlighting specific effects of prolonged and transient neuromodulatory influences on slow brain dynamics.

Keywords: arousal; fMRI; network integration; pupil size; traveling waves.

Introduction

A burning question in neuroscience is how the brain maintains high flexibility to deal with varying demands despite a relatively fixed anatomical structure. To answer this question, the growing field of brain dynamics has moved beyond "static" to more dynamic, time-resolved measures of functional connectivity (Iraji et al. 2021). An important conclusion from this research is that, over the course of an experiment, patterns of functional connectivity in functional magnetic resonance imaging (fMRI) data fluctuate between periods of network-level integration, characterized by relatively strong interconnections between network modules, and periods of network-level segregation, characterized by relatively high network modularity (Keilholz et al. 2013; Sadaghiani et al. 2015; Betzel et al. 2016; Shine et al. 2016; Shine and Poldrack 2018). The dynamic nature of brain integration is further evidenced by computational modeling, which also indicates that alterations in network integration are tightly related to the functional distinction between brain regions (Fornito et al. 2015; Lord et al. 2017; Wei et al. 2022). However, the properties of global brain activity that drive these state changes remain poorly understood.

Recent research on whole-brain dynamics has revealed the presence of slow "traveling waves" that propagate through the brain following a gradient from unimodal to transmodal areas (Matsui et al. 2016; Gu et al. 2021; Raut et al. 2021; Yousefi and Keilholz 2021). Animal studies suggest that these waves reflect modulations of neuronal spiking activity spanning several seconds (Gu et al. 2021; Yang et al. 2024). Interestingly, it has been suggested that the propagation of activity across this gradient could give rise to some of the hallmark findings in studies of dynamic functional connectivity using fMRI (Raut et al. 2023; Shahsavarani et al. 2023). The identification of correlated networks may be influenced by the position of modules along the continuous gradient underlying observed traveling waves. An untested prediction of this hypothesis is that a change in the speed of propagation must cause variations in the correlation between networks. Specifically, if activity propagates faster, it should result in more temporal alignment between modular time courses, manifested as higher network-level integration. Finding such evidence would underscore the importance of the slow propagation of activity as an organizing principle of brain dynamics, and enhance our understanding of the flexible nature of the brain.

What can cause changes in the propagation speed of traveling waves? One possible factor is the level of neural excitability as set by neuromodulatory systems (Munn et al. 2021; Raut et al. 2023), which act at fast and slow time scales and influence large parts of the brain through their widespread projections (McCormick et al. 2020). Low levels of neuromodulatory tone are related to lower excitability and more neural synchronization, while intermediate levels are related to higher excitability and an overall desynchronization (Aston-Jones and Cohen 2005). A computational study has found that larger excitability is associated with faster traveling waves (Bhattacharya et al. 2021). Empirical

Received: April 9, 2025. **Revised:** June 2, 2025. **Accepted:** June 16, 2025

studies offer indirect evidence, by showing that stimulation of the locus coeruleus (Grimm et al. 2024) and spontaneous changes in pupil size (Shine et al. 2016; Mäki-Marttunen 2021; Lee et al. 2022) are associated with systematic changes in brain integration.

Here, we aimed to directly examine the effect of neuromodulatory tone on global brain activity dynamics and measures of integration in a pharmacological fMRI–pupillometry study. We first detected traveling waves and characterized them in terms of speed, directionality, and ratio of top-down (TD) to bottom-up (BU) propagations. We examined these features during rest and task performance, in relation to pupil size (a measure of neuromodulatory tone; Gilzenrat et al. 2010; Joshi and Gold 2020; Mäki-Marttunen and Espeseth 2021; Lloyd et al. 2023), and after the intake of placebo or atomoxetine. Atomoxetine is a noradrenaline transporter blocker that increases extracellular levels of dopamine and noradrenaline (Swanson et al. 2006; Koda et al. 2010), two neuromodulators that innervate large parts of the forebrain, modulate the slope of neuronal activation functions, and tonically increase the overall level of arousal (Aston-Jones and Cohen 2005). We then studied the relation between traveling waves and the participation coefficient, a graph-based measure of brain integration that is sensitive to fluctuations in neuromodulatory inputs (Shine et al. 2016; Shine 2019; Mäki-Marttunen 2021). Based on the predictions laid out in Mäki-Marttunen (2023), we hypothesized that (i) pharmacologically increased levels of catecholamines would be associated with faster traveling waves, (ii) the faster traveling wave speed would be associated with a more integrated network state, and (iii) the presence of traveling waves would be associated with larger pupil size. Our results provide the first evidence in humans that neuromodulation is related to global brain activity propagation and that traveling waves can explain why the level of integration between functional networks fluctuates over time.

Methods

Participants

Thirty-six individuals (average age: 23 years old, range: 18 to 29 years, 14 male) were recruited and medically screened by a physician for physical health and drug contraindications. The exclusion criteria included standard contraindications for MRI, heart arrhythmia, glaucoma, hypertension, use of antidepressants or psychotropic medication, history of psychiatric illness or head trauma, drug or alcohol abuse, learning disabilities, poor eyesight, smoking more than five cigarettes a day, consumption of more than 24 units of alcohol per week, and pregnancy. All the participants gave written informed consent before the experiment and were compensated with €110. The study received ethical approval from the De Medisch-Ethische Toetsingscommissie Leiden, Den Haag, Delft (METC LDD) (CCMO reference number NL73193.058.20).

Study design and MRI data acquisition

The study had a double-blind placebo-controlled crossover design. In each of two sessions, scheduled 1 week apart at the same time of day, participants received either a single oral dose of atomoxetine (40 mg) or a placebo (microcrystalline cellulose PH 102, visually identical to the drug). This dose of atomoxetine is known to increase pupil size (van den Brink et al. 2016) and salivary alpha amylase levels, a hormonal biomarker of central noradrenergic activity (Warren et al. 2017). Participants had a waiting time after pill ingestion, to allow for atomoxetine concentration to reach peak plasma levels. During the waiting interval, they either practiced the tasks (first session) or engaged in some quiet activity of their choice. Approximately 100 min after pill ingestion, participants underwent a resting-state scan, then performed one of the two tasks, underwent another resting-state scan, and performed the second task. The order of the two tasks was counterbalanced across participants.

All the MRI data were collected with a Philips 3T MRI scanner. At the beginning of each of the scanning sessions, we collected a high-resolution anatomical T1 image (echo time 3.5 ms, repetition time 7.99 ms, flip angle 8°, and field of view (FOV) 250 × 195 × 170 mm with voxel size of 1.1 mm isotropic). Functional scans consisted of T2*-weighted echo-planar imaging (EPI) images (echo time 30 ms, repetition time 2.2 s, flip angle 80°, FOV 220 × 220 × 120 mm with voxel size 2.75 mm isotropic). Eye-tracking data were collected during the fMRI scans using an MRI-compatible EyeLink device. The camera was set to image the right eye and a calibration was carried out soon after the participant entered the scanner. The eye-tracking recordings were sampled at a frequency of 1000 Hz.

Tasks and stimuli

In the scanner, participants underwent two resting-state fMRI runs, and performed one run of a continuous performance task and one run of a movie-watching task. During the resting-state scan, participants were instructed to fixate their eyes on a black cross on a gray background. In the continuous performance task, they were presented with a stream of images of cities and mountains and had to mentally count the number of pictures with mountains. The stimuli consisted of 10 pictures of cities and 10 pictures of mountain landscapes that were presented multiple times in random order across the run. A key characteristic was that the transition between images was softened by making images fade into the next, which ensured a "continuous" type of stimulation. The images subtended approximately 6° of visual angle, were isoluminant, grayscaled, and presented on a gray background. The images linearly and continuously morphed from one into the next, with an 800-ms interval (van den Brink et al. 2016). The percentage of mountains in the first session was set to 10% and on the second session to 40%. After the run, participants were asked how many mountains they had counted. The participants also performed a naturalistic viewing task, which involved watching a shortened version of Hitchcock's episode "Bang." This clip has been widely used in fMRI experiments because it includes moments of suspense associated with specific brain patterns that can be observed across individuals (Naci et al. 2014). The clip included sound and subtitles. The resting-state runs and task runs lasted approximately 8 min. The tasks were coded with Psychtoolbox running on MATLAB.

Pupillometry preprocessing and analysis

Raw eye-tracking data were converted to .asc files using the EDF2ASC converter. Preprocessing of the pupil signal consisted of interpolation of pupil blinks, normalization, detrending, and downsampling to the scanner frequency. Coding of these steps was based on code provided by Urai et al. (2017). Cross-correlation between pupil size and global signal was calculated with the function xcorr (MATLAB) as c = xcorr(global signal, pupil). We also identified pseudoevents in the resting-state pupil data, using the point process approach implemented in the rsHRF toolbox (Wu et al. 2021). Briefly, the tool identifies the time points where the signal exceeds 1 standard deviation from the mean and fits an impulse response function. Thus, the "pupil events" are defined as transient pupil changes that resemble an evoked response identified around points of high pupil signal. The rsHRF toolbox allowed us to get the time points at which pupil events were

detected. We calculated the proportion of pupil pseudoevents per time length of the intervals around global signal peaks (see below), because slower waves are expected to be related to longer intervals that may include more pupil events.

fMRI preprocessing and analysis

Data were preprocessed using a standard pipeline implemented in fMRIPrep (Esteban et al. 2019; fmriprep.org), including slice-time correction, image realignment, deconfounding of movement regressors and the mean signal of white matter and cerebrospinal fluid, detrending, and normalization to MNI space. Further steps included filtering (0.001–0.1 Hz) and z-scoring of the voxels' time courses. The analysis of brain activity propagation was done in surface space.

To study brain activity propagation along the principal gradient, we followed the procedure by Gu et al. (2021) and adapted the code shared by the authors. Briefly, the approach consists of, first, identifying the peaks of the global signal and the intervals around each of these peaks (i.e. from the trough before to the trough after each peak), and second, obtaining the time difference between peaks in the time courses of the voxels with respect to the peak in the global signal, that is, the delay values (Fig. 1a and b). The vectors of delay values for all the participants and scans were entered into a singular value decomposition algorithm. We then examined the first five main components (Fig. 1c and d) and identified the one corresponding to the principal gradient, that is, the one where brain regions are organized following a unimodal–transmodal gradient (Fig. 1f). Figure 1e shows the correlation between the vectors of delay values for all the intervals considered and the vector corresponding to the principal gradient component. A bimodal distribution with a higher number of values in negative and positive correlations as compared to no correlation (zero value) indicates the presence of traveling waves in BU and TD directions along the gradient, respectively.

To study activity propagation along this gradient, for each individual and run, the voxels were ordered according to the gradient (i.e. from unimodal to multimodal) and binned in 30 bins to reduce the dimensionality of the analysis. The blood oxygen level-dependent (BOLD) signal for each bin (i.e. averages over voxels) was used to study traveling waves (see a participant's data example in Fig. 1g). Following Gu et al. (2021), we based the analyses on intervals of global involvement, for example those intervals where the global signal (averaged over all gray matter voxels) was larger than the peaks identified from a null distribution (i.e. based on shuffled data). To compute the speed of the waves, we used the formula as in Gu et al. (2021):

$$\text{speed} = |c| \times \text{geodesic distance (mm)}/n \text{ bins/TR (s)},$$

where the coefficient c corresponds to the linear fit where the position of the peak in the BOLD signal for each bin is regressed against the bin number. A positive coefficient corresponded to a propagation from unimodal to transmodal areas (BU), and a negative coefficient corresponded to a propagation from transmodal to unimodal areas (TD). Figure 1h shows the average traveling waves in each direction. We set a threshold for the identification of traveling waves based on the distribution of coefficients for the two other propagation directions (anterior–posterior [A–P] and dorsal–ventral [D–V]). The threshold was set at alpha = 0.1 and corresponded to a coefficient of absolute value 3.8 (Fig. 1i).

For the calculation of brain topological variables, we used the Gordon 333 parcellation (Gordon et al. 2016; Fig. 4d). In the Gordon 333 parcellation, each parcel is assigned to 1 of 12 different networks: Default, Parieto-Occipital, Fronto-Parietal, Salience, Cingulo-Opercular, Medial-Parietal, Dorsal-Attention, Ventral-Attention, Visual, Somatomotor hand, Somatomotor mouth, and Auditory. To account for the fact that the waves were related to peaks in global signal, which could inflate the estimation of integration measures, the global signal was regressed out from each voxel's time course. Data from all the voxels within a parcel were averaged. The temporal segments corresponding to the intervals with traveling waves were used to calculate the correlation coefficient for each pair of parcels, resulting in a connectivity matrix. The 12 networks were used as modules for the calculation of the participation coefficient, a measure of network integration. The participation coefficient was calculated as the average of the weights of a given parcel to each module with respect to all the weights of the parcel. The participation coefficient thus quantifies the extent to which a given parcel connects with parcels in other modules relative to parcels in its own module (van den Heuvel and Sporns 2013). A low participation coefficient corresponds to most of the connections of a parcel being distributed across a single or a small number of modules, while a high participation coefficient corresponds to connections of a parcel being distributed over a large proportion of modules. Therefore, the mean participation coefficient can be used to estimate the extent of integration of the entire brain network. For calculating the participation coefficient, we used the Brain Connectivity Toolbox (Rubinov and Sporns 2010; sites.google.com/site/bctnet).

Experimental design and statistical analyses

We were interested in the effects of treatment (atomoxetine vs placebo) and behavioral state (rest vs task-engaged) on traveling waves, and so we combined the data for the two resting-state scans and compared them with the aggregated data from the two tasks. Data for all detected traveling waves for each individual were used in the analyses. To account for repeated measurements of traveling waves across different treatments and behavioral states, we utilized linear models in MATLAB using the fitlme function. We ran two models with the propagation speed or the TD to BU ratio as the respective dependent variable and treatment and behavioral state as fixed effects. For the analysis of propagation speed, we also included the wave direction (TD vs BU) as an additional factor. To account for the nonindependence of observations within individuals, participant was included as a random effect. For the analysis of pupil-linked arousal, we employed a linear model with mean pupil size in a given time interval as the dependent variable and the presence/direction of traveling waves (none, BU, TD) as the predictor of interest. We also included the treatment and behavioral state as fixed effects and participant as a random effect. To test for a relation between propagation speed, mean pupil size, number of pupil pseudoevents (underlying the resting-state pupil signal), and measures of network-level integration, we ran linear models for each pair of variables. We included treatment and behavioral state as additional predictors and participant as a random effect. In these analyses, we included all the intervals, not only those of significant global involvement, so the correlations covered the whole range of variation in the pupil and integration variables. The linear models were coded using the fitlme function in MATLAB.

Results

Effects of atomoxetine and behavioral state on brain activity propagation

We first confirmed the presence of activity propagation over the whole brain based on activity delays (Gu et al. 2021; Raut et al.

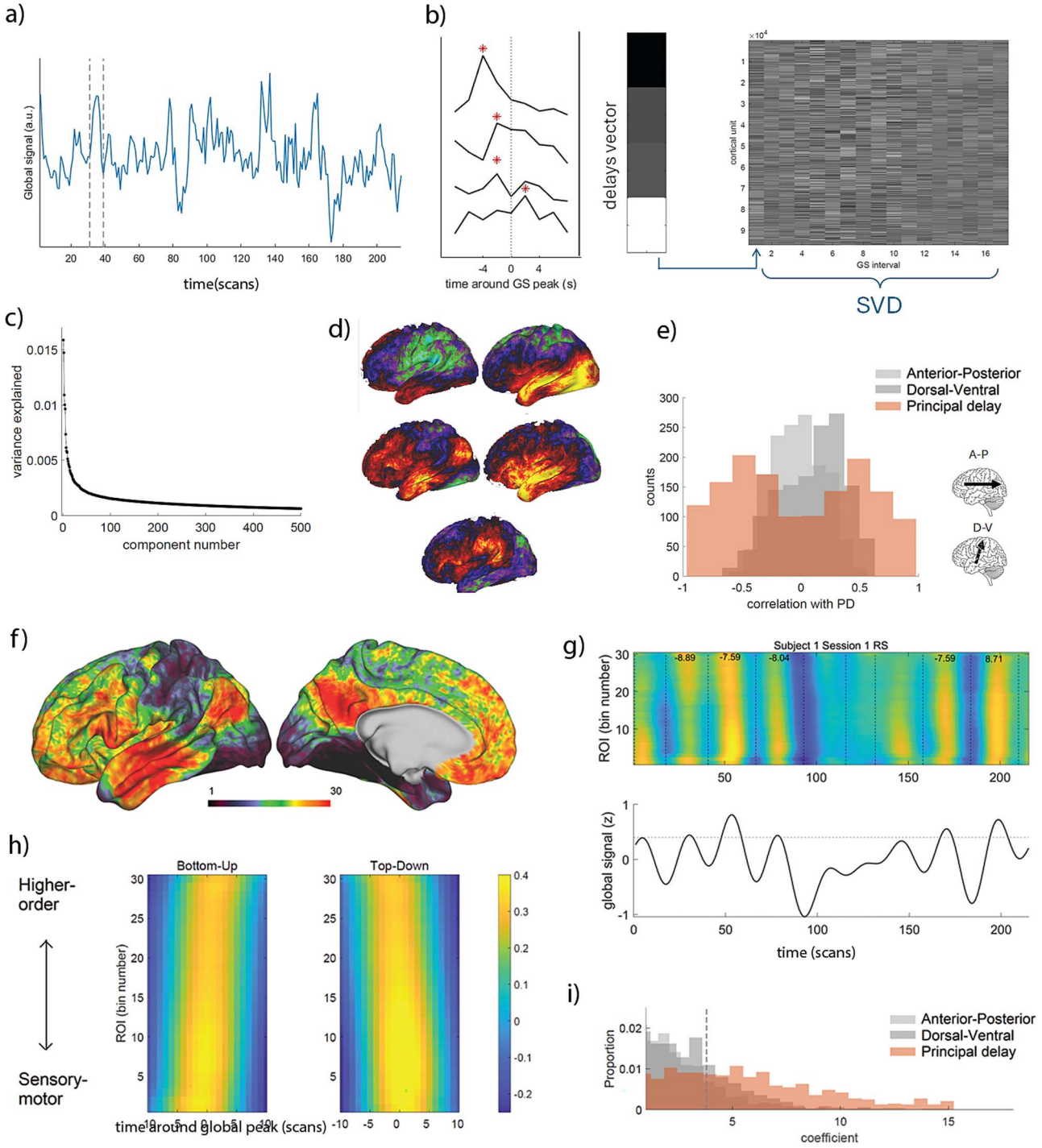

Fig. 1. Overview of methodology for identification of traveling waves. a) Example of extraction of delay vector from one session. b) The peaks of the global signal were identified (left) and the time difference between the peak of activity of each voxel and the global peak were calculated, resulting in one vector of delay values per interval (middle). The delay vectors were concatenated for all participants, sessions, and tasks (right), and the matrix was submitted to a singular value decomposition analysis. c) Variance explained by each component. d) Brain maps corresponding to the first five components. The left map in the middle row (component #3) corresponds to the principal gradient. e) Histogram of correlation values between the delay vectors and the main delay component. The histograms corresponding to the anterior–posterior (A–P) and dorsal–ventral (D–V) gradients are also plotted. Brain insets indicate A–P and D–V directionality. f) Map of principal delay component, binned into 30 bins according to delay with respect to the global signal peak. g) Example of one participant's scan for which we plotted the BOLD signal of the regions of interest ordered after the principal delay (top panel). The traveling waves can be observed in relation to the global signal peaks (bottom panel). The horizontal line indicates the significance threshold for global signal peaks obtained from permutation testing. h) Bottom-up and top-down traveling waves averaged across participants and conditions. i) Distribution of traveling wave coefficients for the two control directions and the principal delay direction. The threshold obtained from permutation testing is indicated with a vertical dashed line.

Table 1. Effects of treatment and behavioral state on traveling waves.

	Speed		TD:BU ratio	
Effect	***F***	***P* value**	***F***	***P* value[a]**
Behavioral state	1.28	0.257	10.54	**0.001**
Treatment	5.61	**0.018**	3.39	0.068
Direction	1.96	0.16		
Treatment × behavioral state	0.19	0.661	0.01	0.907
Behavioral state × direction	0.18	0.670		
Treatment × direction	0.04	0.828		

Abbreviations: BU, bottom-up; TD, top-down. [a]Values in bold are significant at $p = 0.05$.

2021). Briefly, we defined intervals around peaks in the global signal and calculated the delay values of each voxel with respect to the global signal peak (delay profile, Fig. 1a and b). Following singular value decomposition, we identified the prinicipal gradient in these profiles from unimodal to transmodal areas (Fig. 1f; Fig. 1e displays the distribution of correlation values between the delay profiles and the principal gradient). BU and TD waves of activity propagation over the main delay profile in those intervals were then visualized (Fig. 1g and h).

To test our hypothesis that pharmacologically increased levels of catecholamines would be associated with faster traveling waves, we compared the propagation speed of BU and TD waves in the various conditions by performing a repeated-measures ANOVA (RM-ANOVA) with the within-subject factors treatment, behavioral state, and wave direction (BU and TD). This analysis yielded a significant treatment effect [$F(252) = 5.61$, $P = 0.018$, Table 1]. Speed was faster under atomoxetine compared to placebo (Fig. 2a and b, Table 1), confirming our hypothesis. We found no effect of behavioral state or wave direction. Next, we compared the ratio of TD to BU traveling waves between conditions. Figure 2c shows the correlation of traveling waves with the principal delay component: A positive correlation represents a BU direction of propagation while a negative correlation represents a TD direction. The TD-to-BU ratio significantly differed between behavioral states [$F(110) = 10.50$, $P = 0.001$], with a smaller TD:BU, i.e. relatively more BU waves, during task performance than rest (Fig. 2d). The ratio was numerically lower under atomoxetine compared to placebo, but this effect was not significant (Table 1).

To assess the robustness of our finding that atomoxetine speeds up traveling waves, we performed the same analyses in an independent resting-state fMRI–atomoxetine dataset ($N = 26$; van den Brink et al. 2016). The results replicated our finding of the higher speed of traveling waves under atomoxetine (Fig. S1 and Table S1).

Relationship between brain activity propagation and pupil-linked arousal

To study the relation between pupil size and brain dynamics, we investigated the slow fluctuations in the pupil signal filtered with the same band-pass filter as the BOLD global signal (0.001 to 0.01 Hz). These pupil-size fluctuations reflect slow changes in the activity of neuromodulatory nuclei (Joshi and Gold 2020; Mäki-Marttunen and Espeseth 2021; Lloyd et al. 2023). Examples of temporally aligned traveling waves and the global signal and pupil signal for a resting-state session of one participant are displayed in Fig. 3a. We found that atomoxetine was associated with an overall increase in mean pupil size (Fig. 3b), consistent with previous studies (van den Brink et al. 2016) and offering an indication of the efficacy of the pharmacological manipulation. We found that the global signal and the filtered pupil signal were cross-correlated with a lag of around −5 scans (11 s), with fluctuations in the global signal preceding the corresponding fluctuations in pupil size (Fig. 3c). This direction is consistent with previous reports (Bolt et al. 2025). The presence of several significant intervals may show certain periodicity in the signals. The cross-correlation was largely consistent across behavioral states and treatments. We also investigated pupil pseudoevents, that is large (i.e. seemingly evoked), changes in the resting-state pupil signal (Fig. 3d; see Methods). We assumed that these were time points associated with phasic bursts of activity in neuromodulatory nuclei, including the locus coeruleus (Munn et al. 2021). The pseudoevents were only obtained in the resting-state scans to avoid stimulus-related pupil changes. We found that the pseudoevents clustered around global signal peaks, and in particular after the peak (Fig. 3e).

To test our hypothesis that the presence of traveling waves would be associated with larger pupil size, we compared intervals with (BU or TD) and intervals without traveling waves. We found a significant effect, with larger pupil size in intervals with BU or TD traveling waves [Fig. 4a; presence of waves effect: $F(277) = 4.19$, $P = 0.041$], confirming our hypothesis. Note that the variability of mean pupil size was also larger for intervals with traveling waves. We then tested the relation between our pupil-related variables (mean pupil size and proportion of pseudoevents; Fig. 4b and c) and propagation speed. Propagation speed was not associated with mean pupil signal [$F(1,034) = 0.05$, $P = 0.822$] but was significantly associated with proportion of pseudoevents [$F(471) = 4.40$, $P = 0.036$], whereby intervals with larger propagation speed were associated with less pseudoevents. No differences between conditions were observed in these analyses (mean pupil, treatment effect: $F = 0.12$, $P = 0.723$, behavioral state effect: $F = 0.02$, $P = 0.877$; pseudoevents, $F = 0.049$, $P = 0.484$). Taken together, the results suggest that time periods with traveling waves were characterized by larger mean pupil-linked arousal, and that speed of traveling waves was negatively associated with the proportion of pseudoevents.

Relation between brain activity propagation and network topology

To test the hypothesis that faster traveling wave speed would be associated with a more integrated network state, we calculated the participation coefficient, a measure of network integration. For this, we used the Gordon parcellation that divides up the cortex into 333 parcels (Fig. 4d), and averaged the data from all the voxels within each parcel. Each parcel is assigned to a resting-state network, and this assignment was used to compute the participation coefficient. We found that propagation speed was positively related to the level of integration [Fig. 4f;

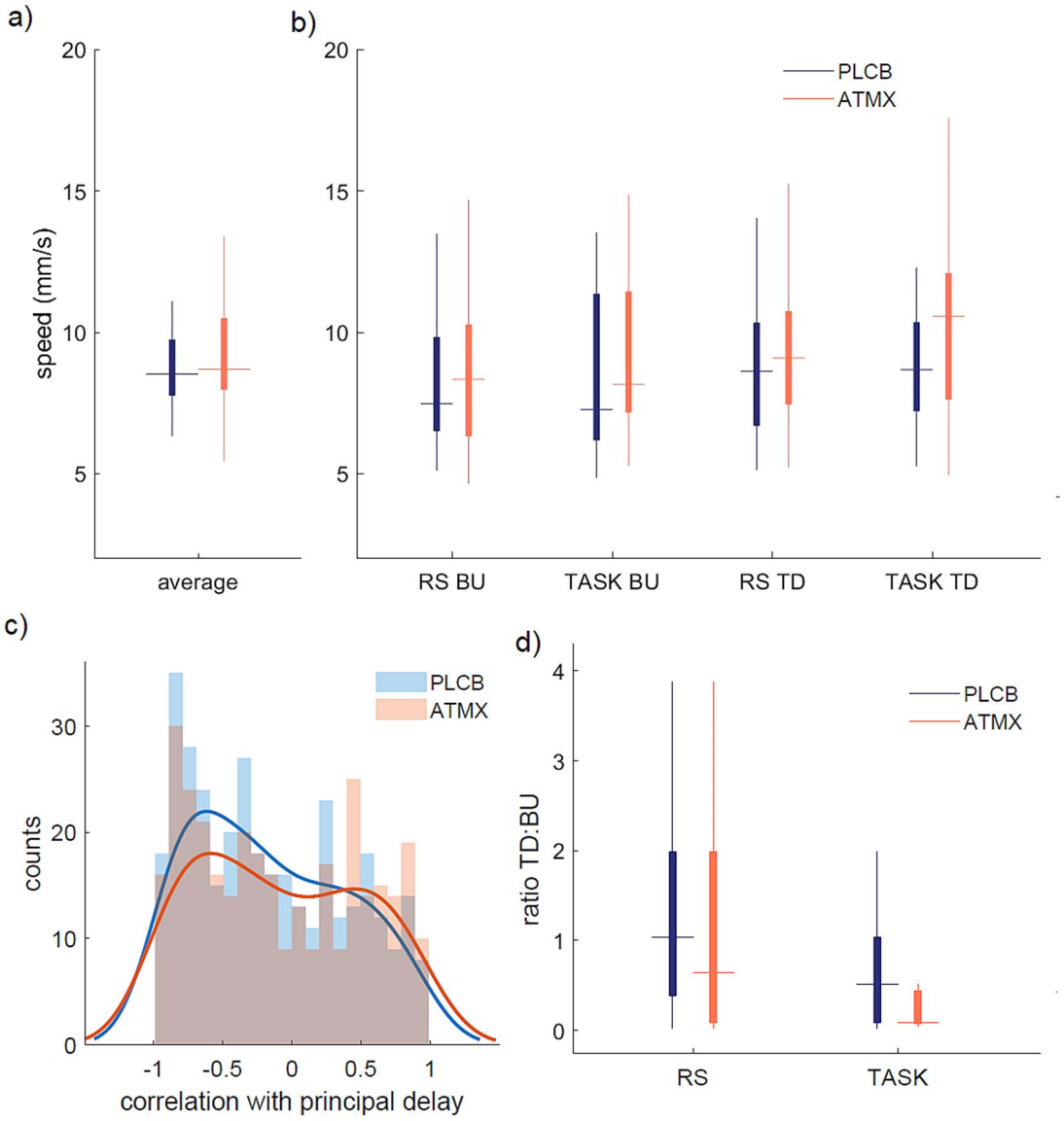

Fig. 2. Traveling wave speed and ratio across treatment and behavioral state. a) Speed of traveling waves in the two treatment conditions and b) separated by treatment, behavioral state, and wave direction. c) Histogram of correlation values between the delay vectors of the individual windows with traveling waves and the principal delay vector. d) Ratio of top-down (TD) to bottom-up (BU) waves per treatment and behavioral state. In the box plots, the central mark is the median, the edges of the box are the 25th and 75th percentiles, and the whiskers extend to the most extreme data points. PLCB, Placebo; ATMX, atomoxetine; RS, resting state.

$F(683) = 97.79$, $P < 0.001$], confirming our hypothesis. There were no significant effects of treatment ($F = 0.01$, $P = 0.925$) and behavioral state ($F = 0.74$, $P = 0.387$) on the level of integration. We also tested for a relation between pupil size and integration. We categorized all the time intervals into four bins on the basis of mean pupil size and tested for an effect on the participation coefficient, following the procedure used in Mäki-Marttunen (2021). We found that larger pupil size was related to higher network integration, with the exception of the largest pupil bin, resulting in an inverted U shape [Fig. 4e; pupil bin linear effect: $F(396) = 14.35$, $P < 0.001$; pupil bin quadratic effect: $F(396) = 13.83$, $P < 0.001$]. This is consistent with the frequently observed quadratic relationships between arousal and performance (Beerendonk et al. 2024; Nieuwenhuis 2024) and between arousal and neural responses (McGinley et al. 2015). In sum, network integration was positively related to propagation speed and pupil size, the latter also presenting nonlinear effects.

Discussion

Propagation of brain activity in the form of traveling waves is a ubiquitous phenomenon of brain activity, but the factors that modulate traveling waves remain uncertain. The current pharmacological fMRI/pupillometry study aimed to investigate whether neuromodulatory tone has an enabling role in global activity propagation and corresponding alterations in dynamic network topology. We found that traveling waves were faster under atomoxetine, that faster traveling waves in turn were related to more network integration, and that traveling waves tended to occur during periods of relatively large pupil size. Our results support the hypotheses that traveling waves underlie, at least in part, the organization of brain activity into functional connectivity networks, that the relationship between neuromodulatory tone and network integration is mediated by changes in the speed of propagation of traveling waves, and that moment-by-moment

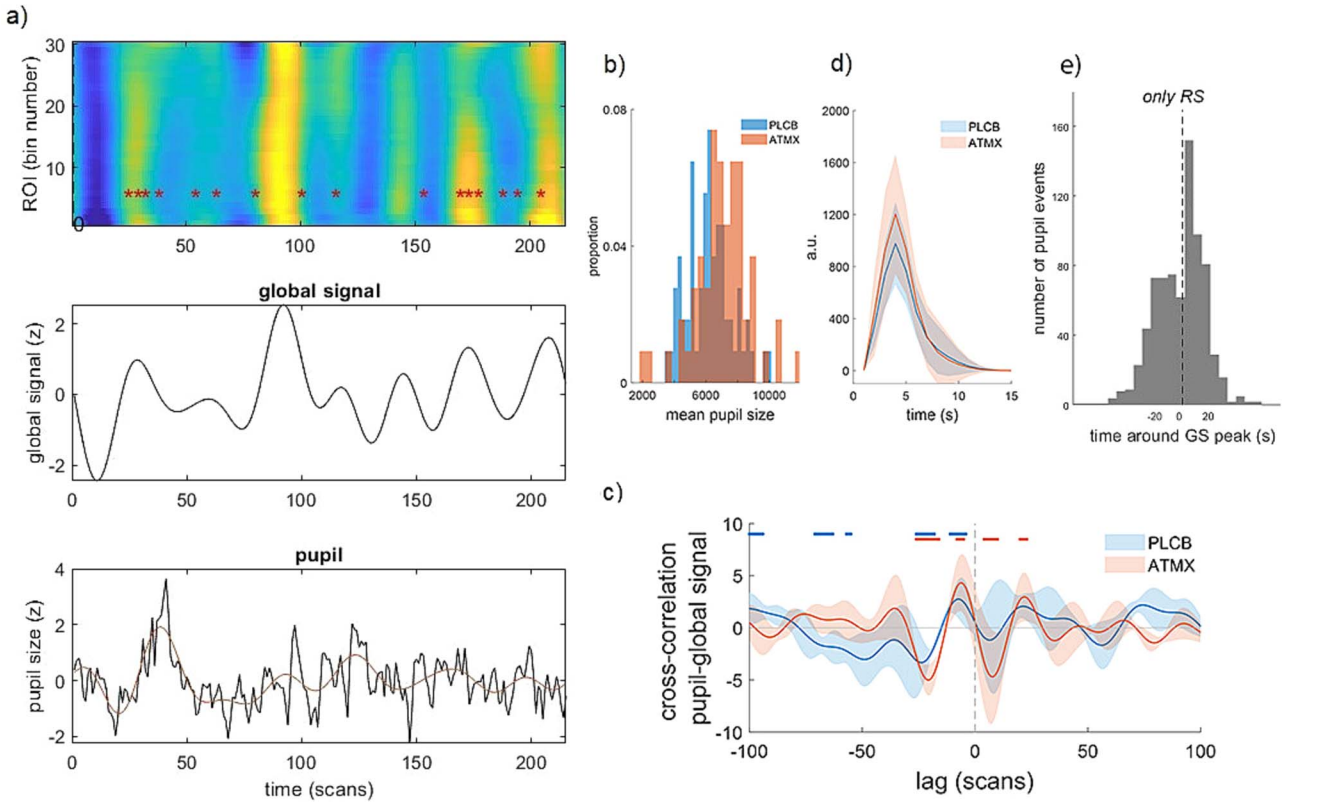

Fig. 3. Relation between pupil size and global signal. a) A sample participant's run. Top panel: brain activity ordered by the principal gradient with identified pupil pseudoevents (estimated from the resting-state pupil data) overlaid as red asterisks. Middle panel: global signal. Bottom panel: pupil signal resampled to the fMRI sampling rate (black) and the low-passed pupil signal (red). b) Histogram of pupil size values for placebo and atomoxetine conditions. c) Average raw cross-correlation between pupil and global signal for the two treatments. PLCB, placebo; ATMX, atomoxetine. d) Average of the phasic pupil changes that were identified as pseudoevents. e) Histogram of distribution of fast pupil events around global signal peaks. RS, Resting state; GS, Global signal.

changes in pupil-linked arousal may enable or facilitate the emergence of global propagation of brain activity. This has important implications for the understanding of the brain mechanisms that underlie the dynamic properties of the human brain.

We examined the presence of traveling waves by extracting a main delay component of the BOLD signal based on intervals determined by global signal peaks and troughs, as has been done previously (Gu et al. 2021). This method allowed us to obtain the main component that reproduces the main gradient of the brain, which separates unimodal from transmodal areas and has been found across perceptual modalities and using various approaches (see Huntenburg et al. 2018 for a review). Replicating Gu et al. (2021), we found both BU and TD propagation of activity. Importantly, we could detect propagating waves in both behavioral states studied here: during rest and during task performance. This is consistent with a previous study that found intrinsic patterns of activity following the principal gradient in the resting state and during a variety of tasks (Brown et al. 2022). An important difference is that in our study none of the tasks required an active motor response or were paced as in event-related designs. Instead, the tasks could be considered as inducing a "continuous" state, which made them comparable with the resting-state runs in terms of design. We found an effect of behavioral state on the traveling wave ratio, where under both atomoxetine and placebo, tasks were associated with a larger proportion of BU traveling waves compared to the resting state. Since the tasks had a strong visual component, it is possible that this effect depended in part on this property of the task (Brown et al. 2022). Other studies found a significantly larger proportion of BU as compared to TD traveling waves in sleepy individuals, as well as in primates (Gu et al. 2021). Furthermore, recent studies using a serotoninergic agonist found that the principal gradient is contracted with increasing levels of serotonin (Girn et al. 2022; Timmermann et al. 2023). Taken together, these results suggest that neuromodulatory factors have an effect on the directionality of propagation of traveling waves along the principal gradient, reflecting the expression of a variety of brain states.

A key finding was that in both behavioral states the speed of traveling waves was significantly higher in the atomoxetine condition. This result was replicated in an independent resting-state data set. Computational studies suggest that one mechanism by which neuromodulatory systems influence the speed of traveling waves is by altering the overall excitability of the brain (Bhattacharya et al. 2021). The noradrenaline and dopamine systems, which are directly affected by noradrenaline transporter blockade with atomoxetine (Bymaster et al. 2002; Swanson et al. 2006; Koda et al. 2010), affect neuronal activity through binding to a variety of receptors distributed over the cortex (Aston-Jones and Waterhouse 2016; Avery and Krichmar 2017; Rho et al. 2018). In particular, atomoxetine increases neuronal excitability (Bymaster et al. 2002; Koda et al. 2010; Di Miceli and Gronier 2015), but it has never been directly tested whether it has an effect on the global, slow propagation of neuronal spiking activity (Liu et al. 2021). Together, these findings suggest that atomoxetine speeds up traveling waves through an increase in neuronal excitability.

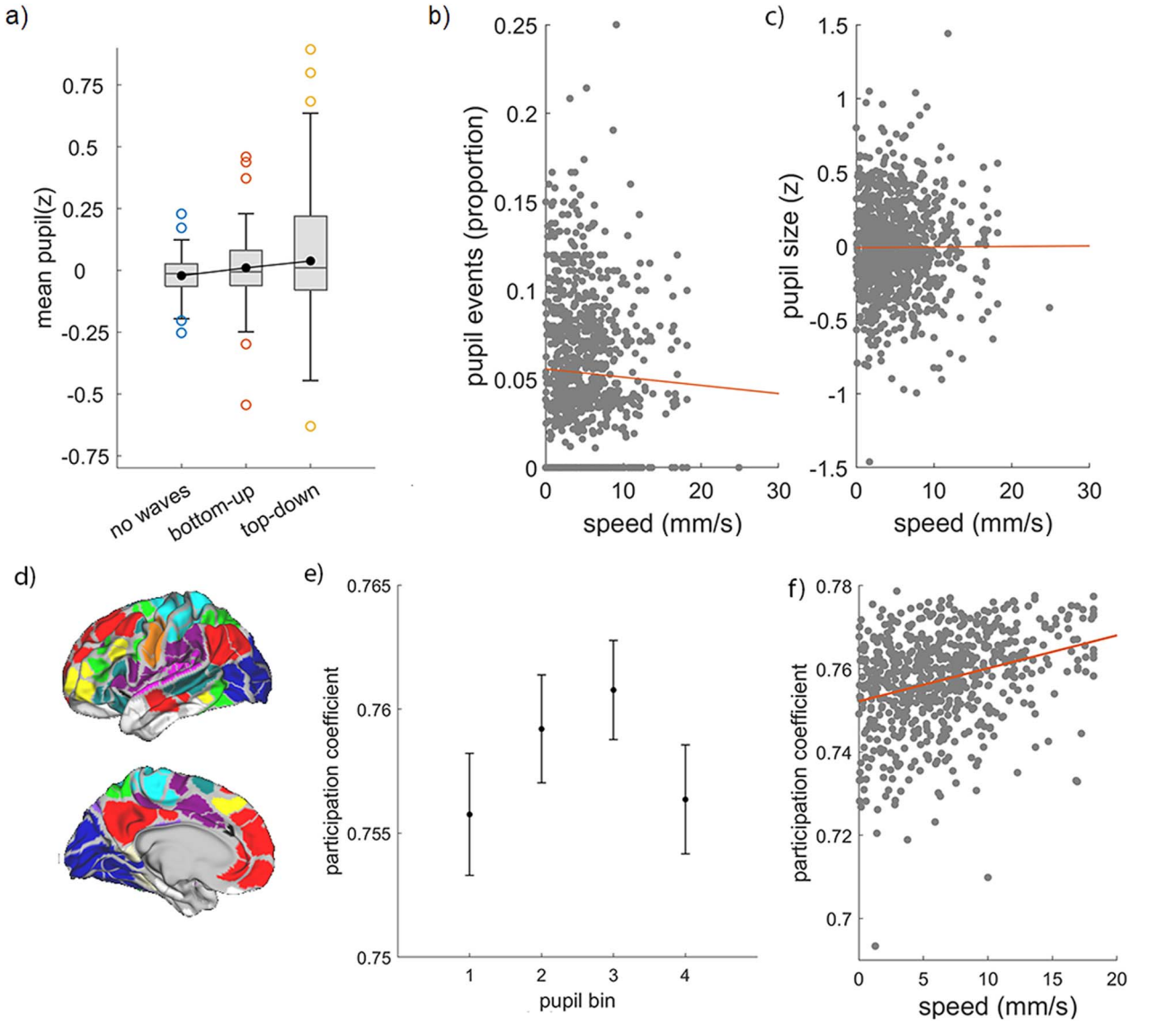

Fig. 4. Links between traveling waves, pupil-linked arousal, and network integration. a) Relation between presence/direction of traveling waves and mean pupil size. b) Relations between propagation speed and pupil measures. Each observation represents one interval of traveling wave. c) Relation between propagation speed and network integration. d) A total of 333 parcels (Gordon et al. 2016) were used to calculate the participation coefficient, a measure of brain integration. e) Relation between pupil size and network integration.

Studies using pupillometry concurrent with fMRI have found that periods of larger pupil size are related to more integration (Shine et al. 2016; Mäki-Marttunen 2021). Atomoxetine manipulation has also been found to affect the brain's integration/segregation balance (Guedj et al. 2016; van den Brink et al. 2016, 2018; Shine et al. 2018). Different measures of brain integration were used across studies, which may underlie some differences in the reported directions of the effect. Our approach allowed us to look at more specific neuromodulatory effects by looking at the traveling waves over the principal gradient. The results revealed that periods of more integration may in part follow changes in the speed of activity propagation across the principal gradient, and these may relate to fluctuations in neuromodulatory tone. Fluctuations between states of network integration and segregation have been described within single scan sessions (Keilholz et al. 2013; Betzel et al. 2016; Shine and Poldrack 2018). Furthermore, several studies have reported that there are specific moments that contribute the most to the phenomenon of functional connectivity (Tagliazucchi et al. 2012; Liu and Duyn 2013). Our results allow tying together these lines of research by suggesting that (i) the modulation of macroscopic brain activity by neuromodulatory tone may reflect not only genuine changes in the overall state of functional connectivity but also the temporal relation of activity propagation across regions following the unimodal–transmodal hierarchy, (ii) the effects of neuromodulatory activity on brain activity propagation may in turn underlie the fluctuations in functional network topology through modulation of propagating waves, and (iii) the single events of traveling waves may be the ones particularly contributing to the emergence of brain functional connectivity. While future studies are needed to provide further support in favor of these hypotheses, our findings offer a clear picture of task-unrelated neuromodulatory effects on brain communication at slow time scales.

We also found that larger pupil size was related to more integration, although integration dropped at the largest pupil size values, following an inverted-U curve. Thus, at least within a

certain range of pupil size, we replicated a previously reported positive relation between pupil size and network integration, as quantified by the participation coefficient (Mäki-Marttunen 2021; Lee et al. 2022). The broader inverted-U curve linking global network integration to pupil size is consistent with findings that have associated both intermediate pupil size (Beerendonk et al. 2024; Nieuwenhuis 2024) and an increase in network integration (Cohen and D'Esposito 2016) with optimal cognitive task performance. These findings, in turn, reflect the positive effects of moderate tonic locus coeruleus activity on network integration (Wainstein et al. 2021; Grimm et al. 2024) and cognitive performance (Aston-Jones and Cohen 2005). We did not find an effect of pupil size on speed but found a significant negative association between number of pupil pseudoevents and propagation speed. While we can only speculate on the meaning of this finding, it is possible that time intervals of faster traveling waves are related to lower variability in neuromodulatory activity and thus fewer pupil pseudoevents. Although more work is needed to test for a relation between traveling waves and pupil size in other conditions and states, our results point toward a timed relation between neuromodulatory activity and global patterns of brain activity.

We also examined a possible relation between the global signal and pupil size. The physiological meaning of the global BOLD signal is still a matter of debate (Liu et al. 2017). The distinction between neuronal and artifactual sources of global signal changes has great relevance for the consideration of global signal removal as a preprocessing step in functional connectivity studies (Power et al. 2017). Previous studies suggest that the global signal is at least in part related to the arousal level (Wong et al. 2013; Liu et al. 2018). We found a relation between pupil size, pupil pseudoevents, and the global signal. A temporal relation between pupil size and the global signal is consistent with previous reports (Bolt et al. 2025). The fact that pupil size and pupil pseudoevents peaked after the global signal may reflect an event of transient arousal following a drop in arousal (Demiral et al. 2023). Our results contribute to the understanding of global brain phenomena by revealing the specific timing between traveling waves associated with increases in the global BOLD signal and transient changes in pupil-linked arousal.

A point of consideration regards the effects of our manipulation on brain physiology and behavior in terms of the known inverted-U curve that represents the effect of neuromodulatory systems on neural population activity and effortful behavior (Aston-Jones and Cohen 2005). The atomoxetine manipulation likely shifted the basal level of neuromodulatory tone toward a more aroused brain, consistent with increased pupil size (Fig. 3b) and previously reported increases in exploratory behavior and larger overall brain interaction under atomoxetine (Pfeffer et al. 2021). We found that the TD:BU ratio of traveling waves was lower in tasks and also under atomoxetine (although this effect was not significant, $P = 0.068$). These effects may be linked to previous findings that atomoxetine is related to a stronger link between network reorganization and arousal during tasks (Shine et al. 2018; Pfeffer et al. 2021). Our design only allowed us to assess a part of the inverted-U curve (i.e. normal to a large neuromodulatory tone), although our analyses with pupil size indicated that lower arousal was related to lower integration and fewer traveling waves. Together, the results underscore the complex ways in which neuromodulators affect overall brain communication as well as activity in specific circuits. Future studies could determine whether infraslow traveling wave activity is related to shifts in behavior and speed across arousal levels and tasks to offer a comprehensive view on the effects of arousal on brain dynamics.

The specific functions of traveling waves remain to be clarified. While, by eliminating discrete stimuli and the need for motor responses, our task design enabled an unconfounded comparison between resting-state and task runs, it did not permit direct testing of the behavioral effects of traveling waves or integration. A recent study found a relation between traveling waves and memory recall (Yang et al. 2024), suggesting that traveling waves, rather than external stimulation, may reflect some kind of internal reorganization. Given their slow and global nature, they may relate to specific needs of the brain to exert global updates of information at slower time scales, something that resonates with global theories of consciousness (Baars et al. 2021; Luppi et al. 2023). Alternatively, traveling waves may relate to a global reset of functional circuits, which can be linked to early theories of neuromodulatory signals as a "network reset" (Bouret and Sara 2005). Future research should examine the relevance of traveling waves in terms of behavior and network organization. For instance, one approach would be to analyze how permanent and virtual lesions in focal brain areas disrupt normal traveling wave activity and characterizing ensuing alterations in network topology and corresponding cognitive and behavioral deficits (Wei et al. 2022).

Conclusions

The importance of slow activity for brain function and behavior (Greene et al. 2023) and that of pupil size as a readout of the general cortical state (Raut et al. 2023) are increasingly recognized. Our study suggests specific mechanisms that mediate these phenomena by showing that arousal is related to spatiotemporal properties of global activity dynamics. By unveiling a relation between neuromodulatory tone, brain activity propagation along the unimodal–transmodal gradient, and measures of network topology, our study allows linking together several lines of research on brain dynamics and provides new evidence of the effects of prolonged and transient variations of neuromodulatory activity.

Author contributions

Verónica Mäki-Marttunen (Conceptualization, Data curation, Formal analysis, Investigation, Methodology, Software, Validation, Visualization, Writing—original draft, Writing—review & editing) and Sander Nieuwenhuis (Funding acquisition, Project administration, Resources, Writing—original draft, Writing—review & editing).

Supplementary material

Supplementary material is available at *Cerebral Cortex* online.

Funding

This study was funded by the Netherlands Organization for Scientific Research, grant VIC 181.032.

Conflict of interest statement. The authors declare no competing financial interests.

References

Aston-Jones G, Cohen JD. 2005. An integrative theory of locus coeruleus-norepinephrine function: adaptive gain and optimal performance. *Annu Rev Neurosci*. 28:403–450. https://doi.org/10.1146/annurev.neuro.28.061604.135709.

Aston-Jones G, Waterhouse B. 2016. Locus coeruleus: from global projection system to adaptive regulation of behavior. *Brain Res*. 1645:75–78. https://doi.org/10.1016/j.brainres.2016.03.001.

Avery MC, Krichmar JL. 2017. Neuromodulatory systems and their interactions: a review of models, theories, and experiments. *Front Neural Circuits*. 11:108. https://doi.org/10.3389/fncir.2017.00108.

Baars BJ, Geld N, Kozma R. 2021. Global Workspace Theory (GWT) and prefrontal cortex: recent developments. *Front Psychol*. 12:749868. https://doi.org/10.3389/fpsyg.2021.749868.

Beerendonk L et al. 2024. A disinhibitory circuit mechanism explains a general principle of peak performance during mid-level arousal. *Proc Natl Acad Sci USA*. 121:e2312898121. https://doi.org/10.1073/pnas.2312898121.

Betzel RF, Fukushima M, He Y, Zuo X-N, Sporns O. 2016. Dynamic fluctuations coincide with periods of high and low modularity in resting-state functional brain networks. *NeuroImage*. 127:287–297. https://doi.org/10.1073/pnas.2320177121.

Bhattacharya MB, Cauchois PA, Iglesias ZSC. 2021. The impact of a closed-loop thalamocortical model on the spatiotemporal dynamics of cortical and thalamic traveling waves. *Sci Rep*. 11: 1–19.

Bolt T et al. 2025. Autonomic physiological coupling of the global fMRI signal. *Nat Neurosci*. 28:1327–1335. https://doi.org/10.1038/s41593-025-01945-y.

Bouret S, Sara SJ. 2005. Network reset: a simplified overarching theory of locus coeruleus noradrenaline function. *Trends Neurosci*. 28:574–582. https://doi.org/10.1016/j.tins.2005.09.002.

Brown JA, Lee AJ, Pasquini L, Seeley WW. 2022. A dynamic gradient architecture generates brain activity states. *NeuroImage*. 261:119526. https://doi.org/10.1016/j.neuroimage.2022.119526.

Bymaster FP et al. 2002. Atomoxetine increases extracellular levels of norepinephrine and dopamine in prefrontal cortex of rat: a potential mechanism for efficacy in attention deficit/hyperactivity disorder. *Neuropsychopharmacology*. 27:699–711. https://doi.org/10.1016/S0893-133X(02)00346-9.

Cohen JR, D'Esposito M. 2016. The segregation and integration of distinct brain networks and their relationship to cognition. *J Neurosci*. 36:12083–12094. https://doi.org/10.1523/JNEUROSCI.2965-15.2016.

Demiral SB, Kure Liu C, Benveniste H, Tomasi D, Volkow ND. 2023. Activation of brain arousal networks coincident with eye blinks during resting state. *Cereb Cortex*. 33:6792–6802. https://doi.org/10.1093/cercor/bhad001.

Di Miceli M, Gronier B. 2015. Psychostimulants and atomoxetine alter the electrophysiological activity of prefrontal cortex neurons, interaction with catecholamine and glutamate NMDA receptors. *Psychopharmacology*. 232:2191–2205. https://doi.org/10.1007/s00213-014-3849-y.

Esteban O et al. 2019. fMRIPrep: a robust preprocessing pipeline for functional MRI. *Nat Meth*. 16:111–116. https://doi.org/10.1038/s41592-018-0235-4.

Fornito A, Zalesky A, Breakspear M. 2015. The connectomics of brain disorders. *Nat Rev Neurosci*. 16:159–172. https://doi.org/10.1038/nrn3901.

Gilzenrat MS, Nieuwenhuis S, Jepma M, Cohen JD. 2010. Pupil diameter tracks changes in control state predicted by the adaptive gain theory of locus coeruleus function. *Cogn Affect Behav Neurosci*. 10: 252–269. https://doi.org/10.3758/CABN.10.2.252.

Girn M et al. 2022. Serotonergic psychedelic drugs LSD and psilocybin reduce the hierarchical differentiation of unimodal and transmodal cortex. *NeuroImage*. 256:119220. https://doi.org/10.1016/j.neuroimage.2022.119220.

Gordon EM et al. 2016. Generation and evaluation of a cortical area parcellation from resting-state correlations. *Cereb Cortex*. 26: 288–303.

Greene AS, Horien C, Barson D, Scheinost D, Constable RT. 2023. Why is everyone talking about brain state? *Trends Neurosci*. 46:508–524. https://doi.org/10.1016/j.tins.2023.04.001.

Grimm C et al. 2024. Tonic and burst-like locus coeruleus stimulation distinctly shift network activity across the cortical hierarchy. *Nat Neurosci*. 27:2167–2177. https://doi.org/10.1038/s41593-024-01755-8.

Gu Y et al. 2021. Brain activity fluctuations propagate as waves traversing the cortical hierarchy. *Cereb Cortex*. 31:3986–4005. https://doi.org/10.1093/cercor/bhab064.

Guedj C et al. 2016. Boosting norepinephrine transmission triggers flexible reconfiguration of brain networks at rest. *Cereb Cortex*. 27:4691–4700. https://doi.org/10.1093/cercor/bhw262.

Huntenburg JM, Bazin PL, Margulies DS. 2018. Large-scale gradients in human cortical organization. *Trends Cogn Sci*. 22:21–31. https://doi.org/10.1016/j.tics.2017.11.002.

Iraji A et al. 2021. Tools of the trade: estimating time-varying connectivity patterns from fMRI data. *Soc Cogn Affect Neurosci*. 16: 849–874.

Joshi SJ, Gold I. 2020. Pupil size as a window on neural substrates of cognition. *Trends Cogn Sci*. 24:466–480. https://doi.org/10.1016/j.tics.2020.03.005.

Keilholz SD, Magnuson ME, Pan WJ, Willis M, Thompson GJ. 2013. Dynamic properties of functional connectivity in the rodent. *Brain Connect*. 3:31–40. https://doi.org/10.1089/brain.2012.0115.

Koda K et al. 2010. Effects of acute and chronic administration of atomoxetine and methylphenidate on extracellular levels of noradrenaline, dopamine and serotonin in the prefrontal cortex and striatum of mice. *J Neurochem*. 114:259–270. https://doi.org/10.1111/j.1471-4159.2010.06750.x.

Lee K et al. 2022. Arousal impacts distributed hubs modulating the integration of brain functional connectivity. *NeuroImage*. 258:119364. https://doi.org/10.1016/j.neuroimage.2022.119364.

Liu TT, Nalci A, Falahpour M. 2017. The global signal in fMRI: nuisance or information? *NeuroImage*. 150:213–229. https://doi.org/10.1016/j.neuroimage.2017.02.036.

Liu X, Duyn JH. 2013. Time-varying functional network information extracted from brief instances of spontaneous brain activity. *Proc Natl Acad Sci USA*. 110:4392–4397. https://doi.org/10.1073/pnas.1216856110.

Liu X et al. 2018. Subcortical evidence for a contribution of arousal to fMRI studies of brain activity. *Nat Commun*. 9:395. https://doi.org/10.1038/s41467-017-02815-3.

Liu X, Leopold DA, Yang Y. 2021. Single-neuron firing cascades underlie global spontaneous brain events. *Proc Natl Acad Sci USA*. 118:e2105395118. https://doi.org/10.1073/pnas.2105395118.

Lloyd B, de Voogd LD, Mäki-Marttunen V, Nieuwenhuis S. 2023. Pupil size reflects activation of subcortical ascending arousal system nuclei during rest. *ELife*. 12:e84822. https://doi.org/10.7554/eLife.84822.

Lord LD, Stevner AB, Deco G, Kringelbach ML. 2017. Understanding principles of integration and segregation using whole-brain computational connectomics: implications for neuropsychiatric disorders. *Philos Trans R Soc A Math Phys Eng Sci*. 375: 20160283.

Luppi AI et al. 2023. A synergistic workspace for human consciousness revealed by integrated information decomposition. *eLife*. 12:RP88173. https://doi.org/10.1016/j.plrev.2025.04.006.

Mäki-Marttunen V. 2021. Pupil-based states of brain integration across cognitive states. *Neuroscience*. 471:61–71. https://doi.org/10.1016/j.neuroscience.2021.07.016.

Mäki-Marttunen V. 2023. Influence of vigilance-related arousal on brain dynamics: potentials of new approaches. *NeuroImage*. 270:119963. https://doi.org/10.1016/j.neuroimage.2023.119963.

Mäki-Marttunen V, Espeseth T. 2021. Uncovering the locus coeruleus: comparison of localization methods for functional analysis. *NeuroImage*. 224:117409. https://doi.org/10.1016/j.neuroimage.2020.117409.

Matsui T, Murakami T, Ohki K. 2016. Transient neuronal coactivations embedded in globally propagating waves underlie resting-state functional connectivity. *Proc Natl Acad Sci USA*. 113:6556–6561. https://doi.org/10.1073/pnas.1521299113.

McCormick DA, Nestvogel DB, He BJ. 2020. Neuromodulation of brain state and behavior. *Annu Rev Neurosci*. 43:391–415. https://doi.org/10.1146/annurev-neuro-100219-105424.

McGinley MJ, David SV, McCormick DA. 2015. Cortical membrane potential signature of optimal states for sensory signal detection. *Neuron*. 87:179–192. https://doi.org/10.1016/j.neuron.2015.05.038.

Munn BR, Müller EJ, Wainstein G, Shine JM. 2021. The ascending arousal system shapes neural dynamics to mediate awareness of cognitive states. *Nat Commun*. 12:6016.

Naci L, Cusack R, Anello M, Owen AM. 2014. A common neural code for similar conscious experiences in different individuals. *Proc Natl Acad Sci USA*. 111:14277–14282. https://doi.org/10.1073/pnas.1407007111.

Nieuwenhuis S. 2024. Arousal and performance: revisiting the famous inverted-U-shaped curve. *Trends Cogn Sci*. 28:394–396. https://doi.org/10.1016/j.tics.2024.03.011.

Pfeffer T et al. 2021. Circuit mechanisms for the chemical modulation of cortex-wide network interactions and behavioral variability. *Sci Adv*. 7:eabf5620.

Power JD, Plitt M, Laumann TO, Martin A. 2017. Sources and implications of whole-brain fMRI signals in humans. *NeuroImage*. 146:609–625. https://doi.org/10.1016/j.neuroimage.2016.09.038.

Raut RV et al. 2021. Global waves synchronize the brain's functional systems with fluctuating arousal. *Sci Adv*. 7:eabf2709. https://doi.org/10.1126/sciadv.abf2709.

Raut RV et al. 2023. Arousal as a universal embedding for spatiotemporal brain dynamics. *BioRxiv*. 2023.11.06.565918. https://doi.org/10.1101/2023.11.06.565918.

Rho HJ, Kim JH, Lee SH. 2018. Function of selective neuromodulatory projections in the mammalian cerebral cortex: comparison between cholinergic and noradrenergic systems. *Front Neural Circuits*. 12:47.

Rubinov M, Sporns O. 2010. Complex network measures of brain connectivity: uses and interpretations. *NeuroImage*. 52:1059–1069. https://doi.org/10.1016/j.neuroimage.2009.10.003.

Sadaghiani S, Poline J, Kleinschmidt A, D'Esposito M. 2015. Ongoing dynamics in large-scale functional connectivity predict perception. *Proc Natl Acad Sci USA*. 112:8463–8468. https://doi.org/10.1073/pnas.1420687112.

Shahsavarani S et al. 2023. Cortex-wide neural dynamics predict behavioral states and provide a neural basis for resting-state dynamic functional connectivity. *Cell Rep*. 42:112527. https://doi.org/10.1016/j.celrep.2023.112527.

Shine JM. 2019. Neuromodulatory influences on integration and segregation in the brain. *Trends Cogn Sci*. 23:572–583. https://doi.org/10.1016/j.tics.2019.04.002.

Shine JM et al. 2016. The dynamics of functional brain networks: integrated network states during cognitive task performance. *Neuron*. 92:544–554. https://doi.org/10.1016/j.neuron.2016.09.018.

Shine JM, Poldrack RA. 2018. Principles of dynamic network reconfiguration across diverse brain states. *NeuroImage*. 180:396–405. https://doi.org/10.1016/j.neuroimage.2017.08.010.

Shine JM, van den Brink RL, Hernaus D, Nieuwenhuis S, Poldrack RA. 2018. Catecholaminergic manipulation alters dynamic network topology across cognitive states. *Netw Neurosci*. 2:381–396. https://doi.org/10.1162/netn_a_00042.

Swanson CJ et al. 2006. Effect of the attention deficit/hyperactivity disorder drug atomoxetine on extracellular concentrations of norepinephrine and dopamine in several brain regions of the rat. *Neuropharmacology*. 50:755–760. https://doi.org/10.1016/j.neuropharm.2005.11.022.

Tagliazucchi E, Balenzuela P, Fraiman D, Chialvo DR. 2012. Criticality in large-scale brain FMRI dynamics unveiled by a novel point process analysis. *Front Physiol*. 3:15. https://doi.org/10.3389/fphys.2012.00015.

Timmermann C et al. 2023. Human brain effects of DMT assessed via EEG-fMRI. *Proc Natl Acad Sci USA*. 120:e2218949120. https://doi.org/10.1073/pnas.2218949120.

Urai AE, Braun A, Donner TH. 2017. Pupil-linked arousal is driven by decision uncertainty and alters serial choice bias. *Nat Commun*. 8:14637.

van den Brink RL et al. 2016. Catecholaminergic neuromodulation shapes intrinsic MRI functional connectivity in the human brain. *J Neurosci*. 36:7865–7876. https://doi.org/10.1523/JNEUROSCI.0744-16.2016.

van den Brink RL, Nieuwenhuis S, Donner TH. 2018. Amplification and suppression of distinct brainwide activity patterns by catecholamines. *J Neurosci*. 38:7476–7491. https://doi.org/10.1523/JNEUROSCI.0514-18.2018.

van den Heuvel M, Sporns O. 2013. An anatomical substrate for integration among functional networks in human cortex. *J Neurosci*. 33:14489–14500. https://doi.org/10.1523/JNEUROSCI.2128-13.2013.

Wainstein G et al. 2021. The ascending arousal system promotes optimal performance through mesoscale network integration in a visuospatial attentional task. *Netw Neurosci*. 5:890–910. https://doi.org/10.1162/netn_a_00205.

Warren CM, van den Brink RL, Nieuwenhuis S, Bosch JA. 2017. Norepinephrine transporter blocker atomoxetine increases salivary alpha amylase. *Psychoneuroendocrinology*. 78:233–236. https://doi.org/10.1016/j.psyneuen.2017.01.029.

Wei J et al. 2022. Effects of virtual lesions on temporal dynamics in cortical networks based on personalized dynamic models. *NeuroImage*. 254:119087. https://doi.org/10.1016/j.neuroimage.2022.119087.

Wong CW, Olafsson V, Tal O, Liu TT. 2013. The amplitude of the resting-state fMRI global signal is related to EEG vigilance measures. NeuroImage. 83:983–990. https://doi.org/10.1016/j.neuroimage.2013.07.057.

Wu GR et al. 2021. rsHRF: a toolbox for resting-state HRF estimation and deconvolution. *NeuroImage*. 1:118591.

Yang Y, Leopold DA, Duyn JF, Liu X. Propagating cortical waves coordinate sensory encoding and memory retrieval in the human brain. *bioRxiv* 2024.06.24.600438. https://doi.org/10.1101/2024.06.24.600438.

Yousefi B, Keilholz S. 2021. Propagating patterns of intrinsic activity along macroscale gradients coordinate functional connections across the whole brain. *NeuroImage*. 231:117827. https://doi.org/10.1016/j.neuroimage.2021.117827.

Cerebral Cortex, 2025, **35**, bhaf183
https://doi.org/10.1093/cercor/bhaf183
Original Article